



Chemical sintering of Ag nanoparticle conductive inks at room temperature for printable electronics

Bethel Faith Y. Rezaga^{1,2} and Mary Donnabelle L. Balela^{1,*}

¹Sustainable Electronic Materials Group, Department of Mining, Metallurgical, and Materials Engineering, University of the Philippines, Diliman, 1101 Quezon City, Philippines

²Institute of Chemistry, University of the Philippines, 4031 Los Baños, Laguna, Philippines

Received: 9 February 2021

Accepted: 31 May 2021

Published online:
12 June 2021

© The Author(s), under exclusive licence to Springer Science+Business Media, LLC, part of Springer Nature 2021

ABSTRACT

Silver (Ag) nanoparticles with a mean diameter of about 24.3 nm were synthesized by electroless deposition in an aqueous solution using PAA-Na and ascorbic acid as protective and reducing agents, respectively. The Ag nanoparticles were utilized as conductive ink and sintered at room temperature using different halide solutions (NaCl, NaBr, NaI, LiCl, KCl) at varying concentrations. A significant increase in particle size of about 174–990% was observed after sintering depending on the type of halide solution used. This also led to an increase in the electrical conductivity of the printed Ag pattern. Halide solutions with smaller ionic sizes generally promote the fusing of Ag nanoparticles, which results in larger Ag particles (NaCl > NaBr > NaI) and higher electrical conductivity. The use of an ionic stabilizer (PAA-Na salt) is more effective as a capping agent for Ag nanoparticles. Sintering is also more significant in samples stabilized by PAA-Na compared to those with PAA only.

1 Introduction

Printed electronics are products of additive manufacturing technologies, which combine various electronic materials and printing processes [1, 2]. This technology has the potential to revolutionize the fabrication of many electronic and optoelectronic devices, such as thin-film transistors [3], photovoltaics [4, 5], antennas [6, 7], membrane switches [8], and OLED displays [9, 10], leading to more sustainable manufacturing. An important component of printed electronic devices is the conductive ink, which is formulated to be printable on different

substrates including plastics, paper, glass, metal, or fabrics. Recently, metal nanoparticle inks dispersed in a carrier solvent are directly printed on plastic substrates to serve as electrical connectors [11–13].

Conductive metallic inks are commonly made from copper (Cu), gold (Au), and silver (Ag). Among the three, Cu is the most economical and abundant. However, Cu nanoparticles are easily oxidized in an ambient environment, which results in diminishing conductivity over a short amount of time [13–15]. Au is highly conductive and stable against oxidation even at high temperatures. However, Au is a precious metal, which makes Au nanoparticles costly

Address correspondence to E-mail: mlbalela1@up.edu.ph

and not ideal for mass production [16, 17]. Ag, though also a precious metal, is more economical than Au. At the same time, Ag nanoparticles exhibit excellent oxidation resistance [18–21]. Previous studies have also shown that Ag nanoparticles can be easily synthesized in large volumes at low temperatures using liquid-phase methods [12–16, 18, 19]. The cost-effectivity of these synthesis processes for Ag nanoparticles supports the economic advantages of using these nanomaterials in future electronics.

Conductive inks, such as those prepared from Ag nanoparticles, are typically dispersed in aqueous or organic solvents stabilized by polymers and surfactants [22–24]. However, the presence of these stabilizers limits the percolation paths between particles and consequently increases the resistance of the printed pattern. The removal of these organic stabilizers is achieved by sintering at high temperatures [23, 25]. This might be damaging to heat-sensitive substrates. To circumvent this problem, low-temperature sintering methods, such as low-pressure plasma sintering [6], microwave and gamma radiation sintering [25], intense pulse light sintering [20], electron irradiation [26], and chemical sintering [11, 27] have been recently developed.

Previous works have reported different approaches to the chemical sintering of nanoparticles at room temperature. Chemical sintering involves the removal of the polymer stabilizer on the surface of the particles using a fusing solution. In this process, the polymer stabilizer is desorbed from the surface of the metal nanoparticles, leading to destabilization and consequently coalescence. For example, Magdassi et al. sintered Ag nanoparticles at room temperature using poly(diallyldimethylammoniumchloride) (PDAC) as the fusing solution [11]. Room-temperature sintering using PDAC resulted in Ag patterns with sheet resistance and resistivity of 0.05 Ω /square and 6.8 $\mu\Omega$ cm when printed on an Epson photo paper. On the other hand, the sheet resistance and resistivity were 0.68 Ω /square and 70 $\mu\Omega$ cm when printed on a copier paper [11].

Other fusing or sintering agents that have been reported include various halide salts, such as magnesium chloride (MgCl_2) and sodium chloride (NaCl), and some acid halides like hydrochloric acid (HCl) [12, 28, 29]. Similar to PDAC, halide solutions are electrolytic in nature, which could lead to the desorption of polymer stabilizers on the surface of Ag

nanoparticles. In fact, Ag nanoparticle patterns on polyethylene terephthalate (PET) films achieved a conductivity of about 41% of bulk Ag after room-temperature sintering using HCl vapor. Among these studies, the effects of different cations or anions in the halide solutions on the sintering process were not fully discussed. At the same time, chemical sintering was limited to only one type of stabilizer, specifically poly(acrylic) acid sodium salt (PAA-Na). The influence of the type of stabilizer for Ag nanoparticles was also not explored.

In this work, Ag nanoparticles were prepared by electroless deposition (chemical reduction) in an aqueous solution using silver acetate (AgCH_3COO) and ascorbic acid ($\text{C}_6\text{H}_8\text{O}_6$) as Ag precursor and reducing agent, respectively. Poly(acrylic) acid (PAA) and poly(acrylic) acid sodium salt (PAA-Na) were used as stabilizers or capping agents. Two methods of sintering, i.e. (1) direct mixing of Ag nanoparticles and halide solutions and (2) sequential printing of Ag nanoparticles and halide solutions on the substrate, were explored. Different substrates were also used for creating Ag nanoparticle patterns. Further, the effects of the type and concentration of the halide solution (cation and anion) on the sintering of Ag nanoparticles were investigated. Finally, a mechanism for the room temperature sintering of Ag nanoparticles in the presence of halide solutions was proposed. To the best of our knowledge, the mechanism by which the Ag nanoparticles sinter at room temperature in the presence of electrolytic solutions is still not fully explained.

2 Experimental

2.1 Synthesis of Ag nanoparticles by electroless deposition

The synthesis method was based on the reported work by Magdassi et al. [11]. In a typical experiment, Ag nanoparticles were synthesized by adding 4.5 g silver acetate (AgCH_3COO , Sigma Aldrich) and 2.9 g of 20 wt% poly(acrylic) acid sodium salt (PAA-Na MW 8000, Sigma Aldrich) into 28 mL hot distilled water ($\sim 60^\circ\text{C}$) in a reflux set-up. The resulting mixture was heated to 95°C with constant stirring. Once the temperature reached 95°C , 3.4 g of 30 wt% ascorbic acid ($\text{C}_6\text{H}_8\text{O}_6$, Ajax Finechem) was added and the mixture was heated at 95°C with constant

stirring for another 30 min. Afterward, the mixture was cooled down to room temperature and the nanoparticles were collected via centrifugation at 6000 rpm for 90 min. The recovered nanoparticles were washed with distilled water several times and finally dispersed in distilled water for storage. The effect of the nature of surfactant was explored by performing the same synthesis procedure using poly(acrylic) acid (PAA, Sigma Aldrich) as a stabilizer.

2.2 Room temperature sintering of Ag nanoparticles

Two treatments were explored to induce sintering of Ag nanoparticles at room temperature. For treatment 1, sintering of Ag nanoparticles was triggered in the solution by mixing 10 wt% as-prepared Ag nanoparticles in 100 μL of 50 mM aqueous NaCl solution. Then, 20 μL of the resulting mixture was deposited on a cellulose acetate film and air-dried at room temperature for 1 h. For treatment 2, sintering of Ag nanoparticles was initiated after deposition on a substrate by dropping 20 μL of 10 wt% Ag nanoparticles in water. After deposition, the Ag nanoparticles were air-dried at room temperature for 1 h, followed by dropping 20 μL of 50 mM NaCl solution on top of the nanoparticles. The effects of different types and concentration of fusing solutions were investigated using various halide solutions, including sodium chloride (NaCl, EMSURE), sodium bromide (NaBr, Fluka), sodium iodide (NaI, Sigma Aldrich), lithium chloride (LiCl, JT Baker) and potassium chloride (KCl, Horiba) at increasing concentrations (10–75 mM).

2.3 Handwriting of conductive Ag nanoparticle lines

To create conductive Ag lines and patterns, a commercial pen (0.5 mm bold line with 1.0 mm ball, Sakura Gelly Roll Stardust) was used. First, the ink of the commercial pen was blown out using an aspirator. Afterward, the blank pen was immersed in ethanol and sonicated for 1 h for washing. Known amounts of as-prepared and sintered Ag nanoparticle ink formulation were then injected into the cleaned pens. The pen with the Ag nanoparticle ink was then used to handwrite Ag lines and patterns on different substrates.

2.4 Characterization

The surface morphology of the Ag nanoparticles was characterized using scanning electron microscopy (FESEM, Hitachi SU8230). ImageJ (National Institutes of Health (NIH) and the Laboratory for Optical and Computational Instrumentation [LOCI, University of Wisconsin]) was used to measure the dimensions of the nanoparticle. Particle size analysis (Particulate Systems, Nanoplus-1) was also employed to determine the average diameter of the synthesized and fused nanoparticles. Transmission electron microscopy (TEM, JEM-2100F) was also used to confirm the fusing of nanoparticles. The phase composition and crystal structure of the Ag nanoparticles were analyzed by X-ray Diffraction (XRD, Shimadzu XRD-7000) using Cu K α . The handwritten patterns for conductivity measurements were straight lines with lengths and diameters equal to 25 and 2 mm, respectively. One straight line for each halide solution was drawn and the resistance for each line was measured at 10 different points within the line using a digital multimeter (UNI-T UT58A), and the average values with the corresponding standard deviation were reported.

3 Results and discussion

3.1 Room-temperature sintering of Ag nanoparticles

Figure 1 shows the high and low magnification FESEM images of Ag nanoparticles before and after sintering with NaCl at room temperature. The as-prepared Ag nanoparticles are quasi-spherical in shape with an average diameter of 24.3 nm and a relative standard deviation of about 28.9% of the mean as seen in Fig. 1a. This indicates that the as-prepared Ag nanoparticles are relatively monodispersed. This is possibly due to the action of PAA-Na as a stabilizer and capping agent. It was suggested that the interaction between the Ag nanoparticles and PAA-Na is through an Ag-oxygen (Ag–O) bond [29]. The O from the carboxylic group of PAA anchors on the Ag surface in a bidentate mode, probably by ion-dipole interaction [29]. The relative monodispersity of the Ag nanoparticles may be due to the steric hindrance provided by the long polymeric chain of PAA, as well as the electrostatic repulsion of anionic

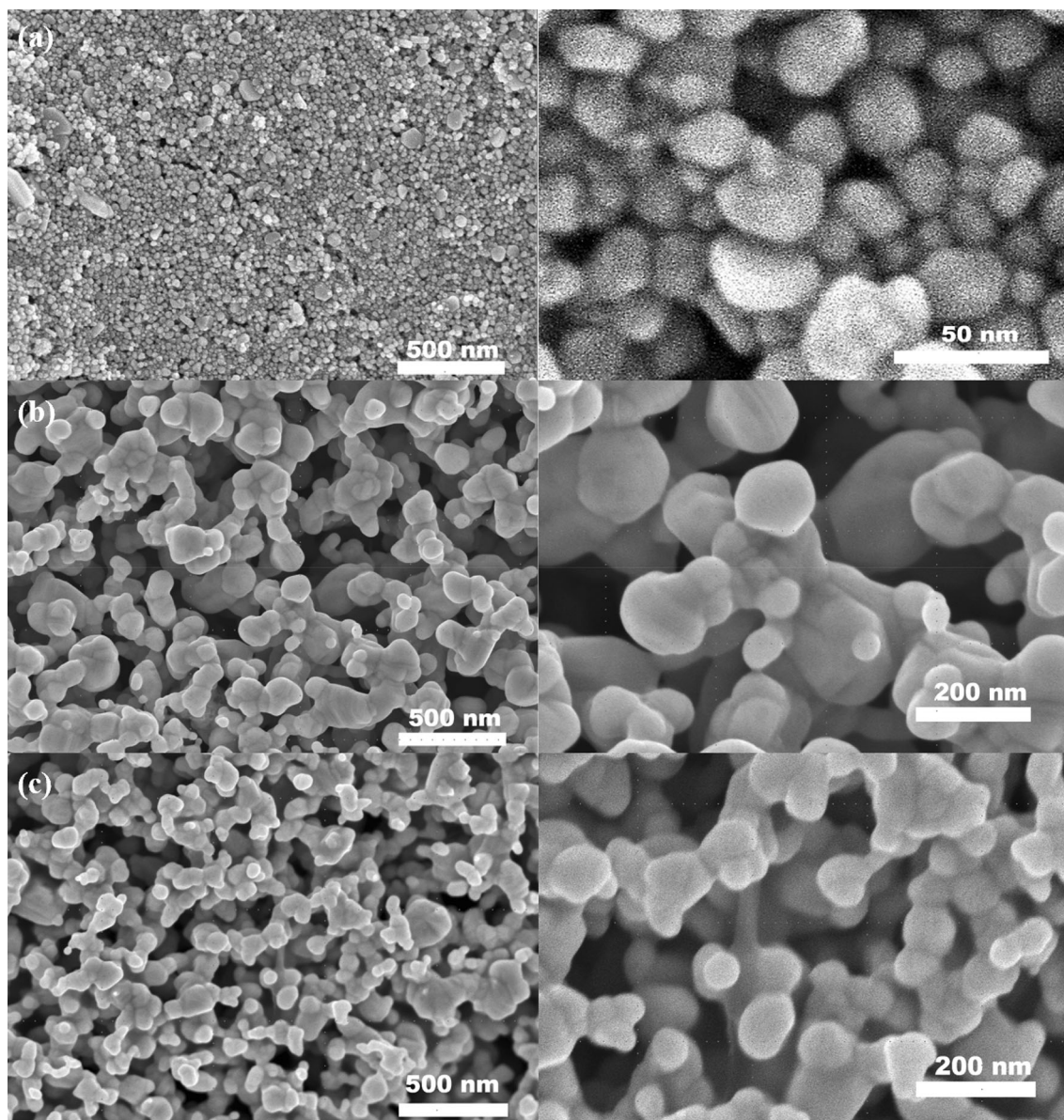


Fig. 1 SEM images of **a** as-prepared Ag nanoparticles, **b** Ag nanoparticles dispersed in 50 mM NaCl solution, and **c** Ag nanoparticles dropped with 50 mM NaCl solution

carboxylic group side chains. Consequently, particle growth and agglomeration of the Ag nanoparticles were hindered.

When the Ag nanoparticles were dispersed in 50 mM NaCl aqueous solution, a drastic increase in the particle size to about 206.5 nm was observed as seen in Fig. 1b. Necks were also formed in between the nanoparticles as seen from the high magnification FESEM image. This could lead to percolation paths for electron movement. Similarly, the particle size was also enlarged when a drop of 50 mM NaCl solution was subsequently added to the printed Ag

nanoparticle ink (Fig. 1c). The average particle diameter was determined to be about 175.1 nm, which is smaller compared to the Ag nanoparticles directly dispersed in NaCl solution. It is possible that the sintering of Ag nanoparticles in solution allows more atom movement among the nanoparticles. Further, diffusion paths might be shorter, which promotes sintering and enlargement of the particle size. On the other hand, the structure of the Ag nanoparticles is more rigid after deposition. Consequently, mass transport is hindered, which limits the sintering process [11, 12, 29]. In both cases, it is clear

that NaCl was effective in inducing the sintering of Ag nanoparticles without heat. Further, there seemed to be a decrease in the total number of Ag nanoparticles present after sintering. This is more apparent in the sample directly mixed with NaCl solution. It is possible that Oswald ripening also played a role in the enlargement of particle size, wherein the smaller Ag nanoparticles were dissolved and deposited on the surface of the larger particles.

The corresponding XRD patterns of the as-prepared and sintered Ag nanoparticles are presented in Fig. 2. Five distinct diffraction peaks at 2θ equal to 38.44° , 44.48° , 65.02° , 77.60° , and 82.20° were identified for all samples. These peaks are due to the reflections of the (111), (200), (220), (311), and (222) planes of face-centered cubic (fcc) Ag (JCPDS File No. 04-0783). No other peaks attributed to AgCH_3COO or any compound were identified from the diffraction patterns of the as-prepared sample in Fig. 2a. This indicates the high purity of the as-prepared Ag nanoparticles. However, extra peaks at 2θ equal to 32.44° and 46.30° were observed for the sintered Ag nanoparticles as seen in Fig. 2b, c. These peaks are attributed to the (200) and (220) planes of AgCl

(JCPDS File No. 31-1238). The Ag halide may be due to the Cl^- ions adsorbed on the surface of Ag nanoparticles, which results in the formation of an AgCl layer. Then again, it is obvious from the XRD patterns that AgCl is only present in minute concentrations and metallic Ag is the predominant phase.

On the other hand, broadening was more pronounced in the diffraction peaks of the as-prepared Ag nanoparticles compared to the sintered samples. This indicates a very small crystallite size of about 6.89 nm determined from the broadening of the (111) peak. This value is smaller than the apparent particle diameter measured from FESEM (24.3 nm), which implies that the Ag nanoparticles are polycrystalline. On the other hand, sharper Ag peaks were observed for the nanoparticles sintered by directly mixing with NaCl as in Fig. 2b. This suggests improved crystallinity possibly due to grain growth after sintering. However, only moderate enhancement in crystallinity was achieved by sintering Ag nanoparticles after printing. These results are consistent with the change in particle size measured from FESEM images in Fig. 1b, c.

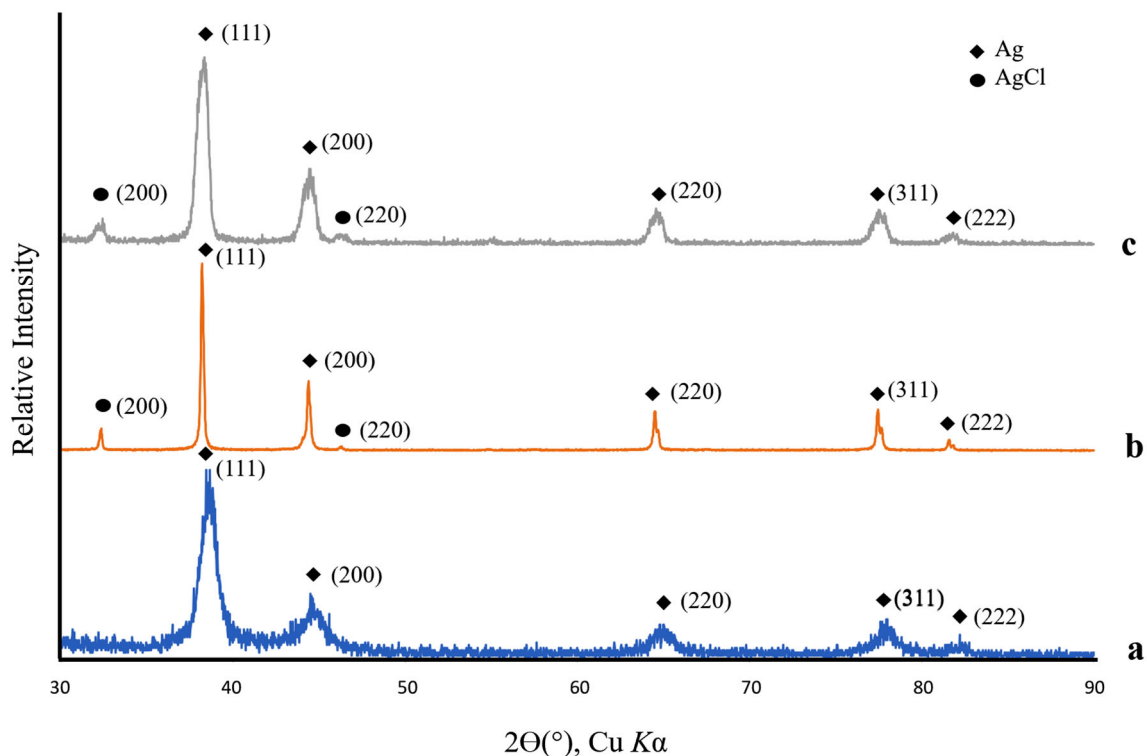


Fig. 2 (Color online) XRD patterns of **a** as-prepared and sintered Ag nanoparticles via **b** mixing with 50 mM NaCl and **c** sequential dropping of Ag nanoparticles and 50 mM NaCl

The electrical resistance of the Ag nanoparticles before and after room temperature sintering on different substrates is listed in Table 1. As-prepared Ag nanoparticles deposited on cellulose acetate achieved an electrical resistance of about 57.7 Ω while deposition on bond paper (80 gsm) resulted in a non-conductive pattern. The Ag nanoparticles were possibly absorbed and deposited in between the cellulose fibers of the paper, which explains the lack of conductive pathways [30]. On the other hand, Ag nanoparticles sintered in a solution of 50 mM NaCl achieved lower resistance (0.3 and 1.3 Ω) after deposition on both substrates. This can be attributed to the increase in particle size after sintering. For the sample sintered by sequential dropping, the measured resistance was about 20.5 and 43.7 Ω for patterns deposited on cellulose and paper, respectively. The apparent decrease in resistance of the Ag patterns is due to the increase in the size of the nanoparticles after sintering. Consequently, an interconnected network of Ag nanoparticles was formed, which led to more conductive pathways [6, 11, 12].

Meanwhile, the porosity and surface roughness of the substrate possibly affect the distance between the Ag nanoparticles after deposition [30]. This then influences the length of the diffusion path during sintering. Compared to bond papers, cellulose acetate films have smaller pore sizes and lower surface roughness. These possibly led to shorter diffusion paths, which promotes the sintering of Ag nanoparticles. As a result, more compact and interconnected Ag nanoparticle patterns were formed on cellulose acetate.

To determine the extent of sintering of Ag nanoparticles, the cross-sectional area of the sintered Ag nanoparticles via sequential dropping was investigated. Figure 3 shows the FESEM images of the cross-section of the sintered Ag nanoparticles

Table 1 Resistance values of as-prepared and sintered Ag nanoparticles using 20 μ L of 50 mM NaCl solution deposited on film and paper

Ag nanoparticles	Resistance, Ω	
	Cellulose acetate	Paper
As-prepared	57.7	–
Sintered via mixing	0.3	1.3
Sintered via sequential dropping	20.5	43.7

after sequential dropping of 10 μ L each of Ag nanoparticles and 50 mM NaCl. It is clear from the FESEM micrograph that sintering did not only occur with the nanoparticles at the surface but progressed to the bottom of the printed pattern. Sintering occurred throughout the whole layer, which indicates that coalescence took place in three dimensions. This large mass transport then results in the densification of the printed Ag nanoparticle pattern [11].

As proof of concept, the 10 wt% Ag nanoparticles dispersed in 50 mM NaCl solution were used to create handwritten patterns on cellulose acetate and bond paper (Fig. 4a, b). The resistance of the sintered Ag nanoparticles was 6.5 and 20 Ω when deposited on cellulose acetate and bond paper, respectively. The patterns were able to light up the LED assembled in a circuit without any annealing and even after bending and folding as shown in Fig. 4c, d. In fact, no significant change in the resistance was observed during the bending/folding test. It was also observed that NaCl improved the adhesion of the Ag nanoparticles onto the plastic substrate. Delamination was observed for samples without NaCl solution, while the sintered pattern remained intact after bending. This may be due to the densification of the sintered nanoparticles, which possibly improved the mechanical integrity.

3.2 Effect of concentration of sintering agent

The effects of different concentrations of sintering agents on the resulting particle size and electrical conductivity were also investigated. NaCl was employed as the model sintering agent. The concentration of aqueous NaCl solution was varied from 10 to 75 mM. The Ag nanoparticle loading was kept constant at 10 wt%, whereas glossy paper was used as substrate. Figure 5 shows the FESEM images of sintered Ag nanoparticles with increasing NaCl concentration. As shown in Fig. 5a, only a few sintered nanoparticles with an average diameter of about 103.7 nm were observed when 10 mM NaCl was used. A low amount of NaCl was possibly not effective in destabilizing the PAA-Na on the surface of the nanoparticles [31].

When the concentration of NaCl was increased to 25 mM, the particle size significantly increased to 195.6 nm as listed in Table 2. However, smaller individual nanoparticles were still present as seen

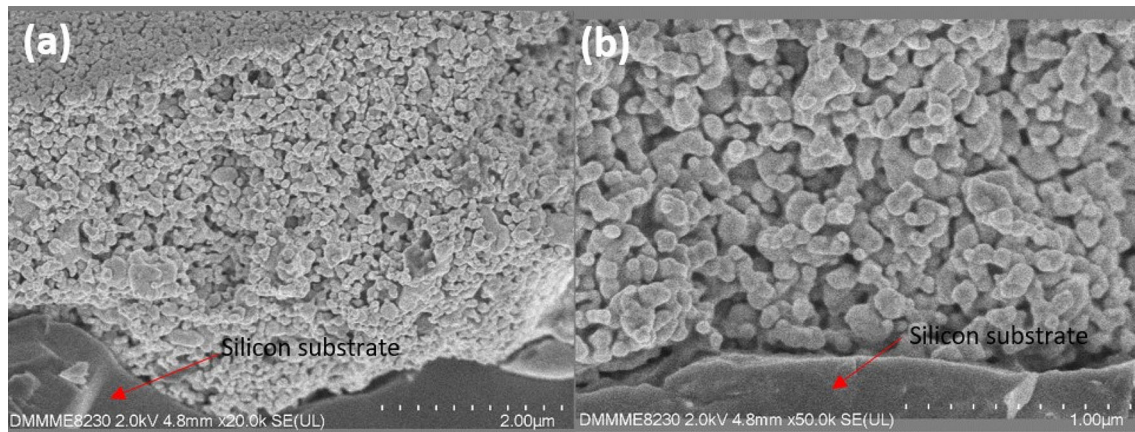


Fig. 3 (Color online) Cross-section SEM images at **a** 20,000 \times and **b** 50,000 \times magnification of sintered nanoparticles via sequential deposition of Ag nanoparticles and 50 mM NaCl solution

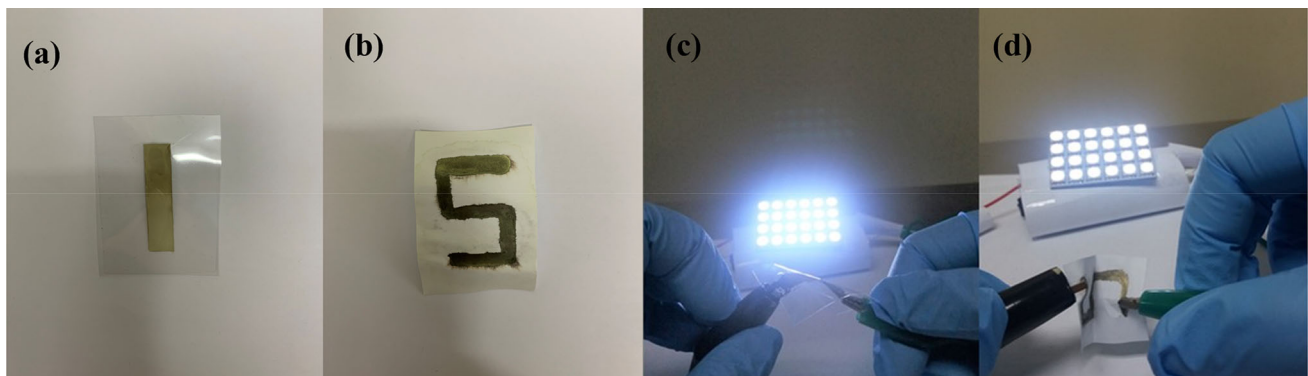


Fig. 4 (Color online) Patterns handwritten on **a** cellulose acetate and **b** bond paper subjected to **c** bending and **d** folding

from Fig. 5b. At 50 mM NaCl, the average particle diameter was measured to be about 197.4 nm. As shown in Fig. 5c, multiple percolation paths between particles were also observed. Necking between particles was clearly present, which confirms the coalescence of individual Ag nanoparticles. Sintering using 75 mM NaCl resulted in very large particles with an average diameter of about 221.7 nm. Almost all of the particles were sintered producing an interconnected network of large particles as seen in Fig. 5d. The presence of a higher number of charged particles, i.e. halide ions, can effectively disrupt the electrostatic stabilization provided by PAA-Na. As a result, the elongated PAA molecules on the surface of Ag nanoparticles were successfully desorbed. Coalescence of Ag nanoparticles then occurred to lower the surface energy.

As more percolation paths were formed at higher concentrations of NaCl, the resistance of the Ag patterns was reduced as seen in Table 2. However, the

large amount of AgCl precipitated on the surface of the sintered Ag nanoparticles, particularly at 75 mM NaCl, might have offset the improvement in the electrical conductivity. It is known that AgCl is non-conductive [30]. Thus, a slight increase in resistance was determined after sintering the nanoparticles with 75 mM NaCl. Though AgCl was precipitated even at lower concentrations of NaCl, their presence might not be sufficient to lower the conductivity of the Ag nanoparticle pattern.

3.3 Effect of type of sintering agent

In addition to NaCl, other halide salts (NaBr and NaI) were used as fusing agents to investigate the effect of type of anion on the sintering process. Figures 5e–l are the FESEM images of Ag nanoparticles sintered with increasing amounts of NaBr and NaI. Similar to NaCl, there is an apparent increase in the size of the particles as the concentrations of NaBr and NaI were

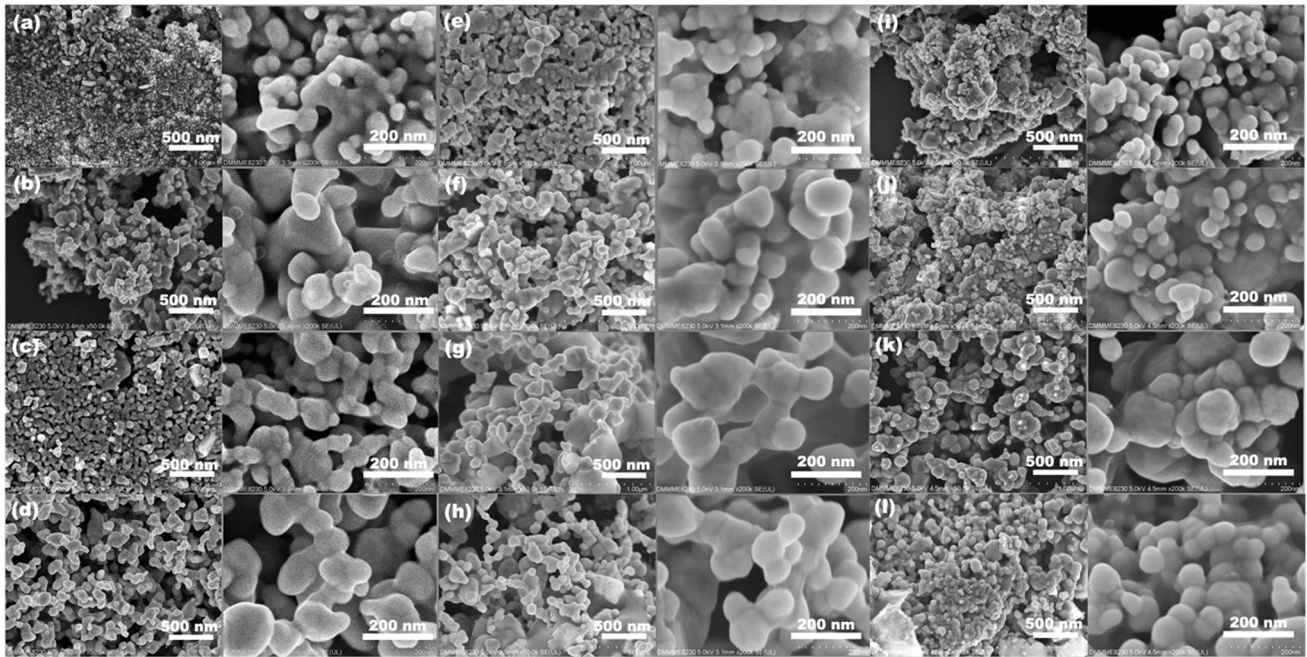


Fig. 5 Ag nanoparticles sintered using **a** 10, **b** 25, **c** 50, and **d** 75 mM NaCl solution, **e** 10, **f** 25, **g** 50, and **h** 75 mM NaBr solution, **i** 10, **j** 25, **k** 50, and **l** 75 mM NaI. The magnification from left to right is 50,000× and 200,000×.

Table 2 Diameter and resistance of Ag nanoparticles fused using halide solutions with different anions handwritten on glossy paper

Ag NP parameters	Fusing solution	Fusing solution concentration, mM				
		0	10	25	50	75
Diameter, nm	NaCl	24	103.7	195.6	197.4	221.7
% increase in diameter		0	332	715	723	824
Diameter standard deviation, %		–	24.55	42.39	19.37	53.75
Resistance, Ω		110,000	216.6	22.9	9.0	16.4
Resistance standard deviation, %		–	103.40	4.10	3.92	8.40
Diameter, nm	NaBr	24	91.5	140.4	187.7	261.6
% increase in diameter		0	281	485	686	990
Diameter standard deviation, %		–	23.23	33.02	38.15	36.41
Resistance, Ω		110,000	406.2	43.0	36.1	–
Resistance standard deviation, %		–	79.32	5.47	7.05	–
Diameter, nm	NaI	24	65.9	101.1	174.5	199.2
% increase in diameter		0	174	321	627	730
Diameter standard deviation, %		–	12.01	27.20	31.38	39.80
Resistance, Ω		110,000	54,360	3297.8	540	2561.2
Resistance standard deviation, %		–	21,055.7	1010.96	146.60	569.20

raised. At 10 mM NaBr, moderate sintering was observed resulting in nanoparticles with an average diameter of 91.5 nm as seen in Table 2. Then again, some free unsintered Ag nanoparticles were still present (Fig. 5e). On the other hand, increasing the NaBr concentration to 25 mM resulted in larger particles of about 140.4 nm. Further increase in NaBr concentration (50 to 75 mM) produced more

significant sintering and improved conductivity. However, Ag nanoparticles sintered using 75 mM NaBr solution could not be printed on cellulose acetate due to severe coagulation and precipitation of crystals, possibly AgBr. As a result, the sintered Ag nanoparticles could not be dispersed in the ink formulation. As seen in the diffraction pattern in Fig. 6a,

AgBr was already present in the sample sintered with 50 mM NaBr.

The efficacy of NaI as a fusing solution was also explored. Low concentrations of NaI (10–25 mM) were also not effective as fusing agents as shown in Fig. 5i–l. As listed in Table 2, the average diameters of Ag nanoparticles were 65.9 and 101.1 nm when 10 and 25 mM NaI were employed, respectively. Increasing the concentration to 50 mM produced particles with an average diameter of 174.5 nm. Necks and multiple percolation paths were also more clearly observed at 50–75 mM NaI. Some crystalline precipitates, i.e. AgI, were also formed after using > 50 mM NaI as seen in the XRD pattern in Fig. 6b. The presence of AgI was also detrimental to the electrical conductivity of the Ag patterns.

To support the SEM results, particle size analysis was performed. Results showed that the Ag particles have an average diameter of 334.8, 321.8, and 262.8 nm when sintered using 50 mM NaCl, NaBr, and NaI, respectively. The largest Ag nanoparticles were obtained after sintering with NaCl, which is more evident at concentrations > 20 mM. This was followed by nanoparticles fused with NaBr, then NaI. The change in particle size due to the anion type can be attributed to the variation in the ionic size of the halide. Cl^- has the smallest ionic radius of about 1.81 Å. On the other hand, Br^- has an ionic radius of about 1.96 Å, whereas 2.20 Å for I^- . The relatively smaller moiety of Cl^- ions compared to Br^- and I^- ions may have efficiently replaced the stabilizer on

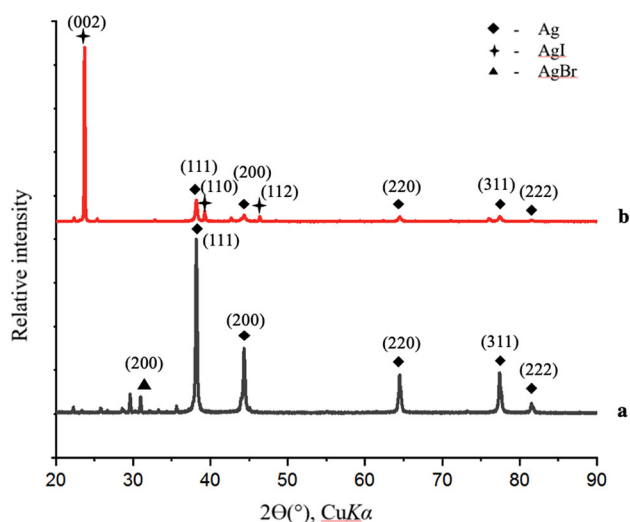


Fig. 6 (Color online) XRD patterns of sintered Ag nanoparticles via mixing with **a** 50 mM NaBr and **b** 50 mM NaI

the surface of the nanoparticles since smaller ions can better penetrate through the elongated polymer on the Ag surface [12]. As more halide ions adsorbed on the surface of the Ag nanoparticles, more PAA molecules were desorbed.

The influence of the type of cation in the halide solution was also studied. Thus, KCl and LiCl were also tested as fusing solutions. Chlorides were chosen as they produced the largest increase in diameter and improvement in electrical conductivity after sintering as discussed in the previous section. Figure 7 presents the FESEM micrographs of Ag nanoparticles sintered at increasing concentrations of LiCl and KCl. As seen in Fig. 7a, an interconnected network of sintered Ag nanoparticles was formed after treating with 10 mM LiCl solution. Necking was also observed, which resulted in multiple percolation paths. As listed in Table 3, particles with an average diameter of 134.8 nm were formed. At 25–75 mM LiCl, significant sintering was observed, leading to a large increase in particle size. However, free Ag nanoparticles were also present as seen in Fig. 7b. Ag nanoparticles were also successfully sintered using KCl solution as shown in Fig. 7e–h. Intense sintering was observed when the KCl concentration was 50–75 mM. The largest increase in particle size (165.8 nm) was observed when 75 mM KCl solution was used as a sintering agent.

It was expected that larger Ag nanoparticles and more conductive Ag patterns will be produced after sintering with LiCl due to its high solubility in water. However, it has been reported that Li^+ ions are more strongly hydrated compared to Na^+ and K^+ [32], which possibly leads to lower mobility in water. In contrast, most alkali metal ions, (e.g. Na^+ and K^+) except Li^+ , are large and their charge densities are low [32, 33]. The electrostatic interactions are also weak and their ability to form covalent interactions is also low due to filled outer electron shells [32]. In particular, potassium is unable to form well-defined hydrate and solvate complexes in the solid-state [32, 33], which indicates weak hydration. Thus, it is possible that larger alkali ions like K^+ are more effective as fusing agents due to their higher mobility in water.

3.4 Proposed sintering mechanism

Figure 8 shows the TEM images of the as-prepared and sintered Ag nanoparticles. The as-prepared Ag nanoparticles have an average diameter of 22.0 nm as

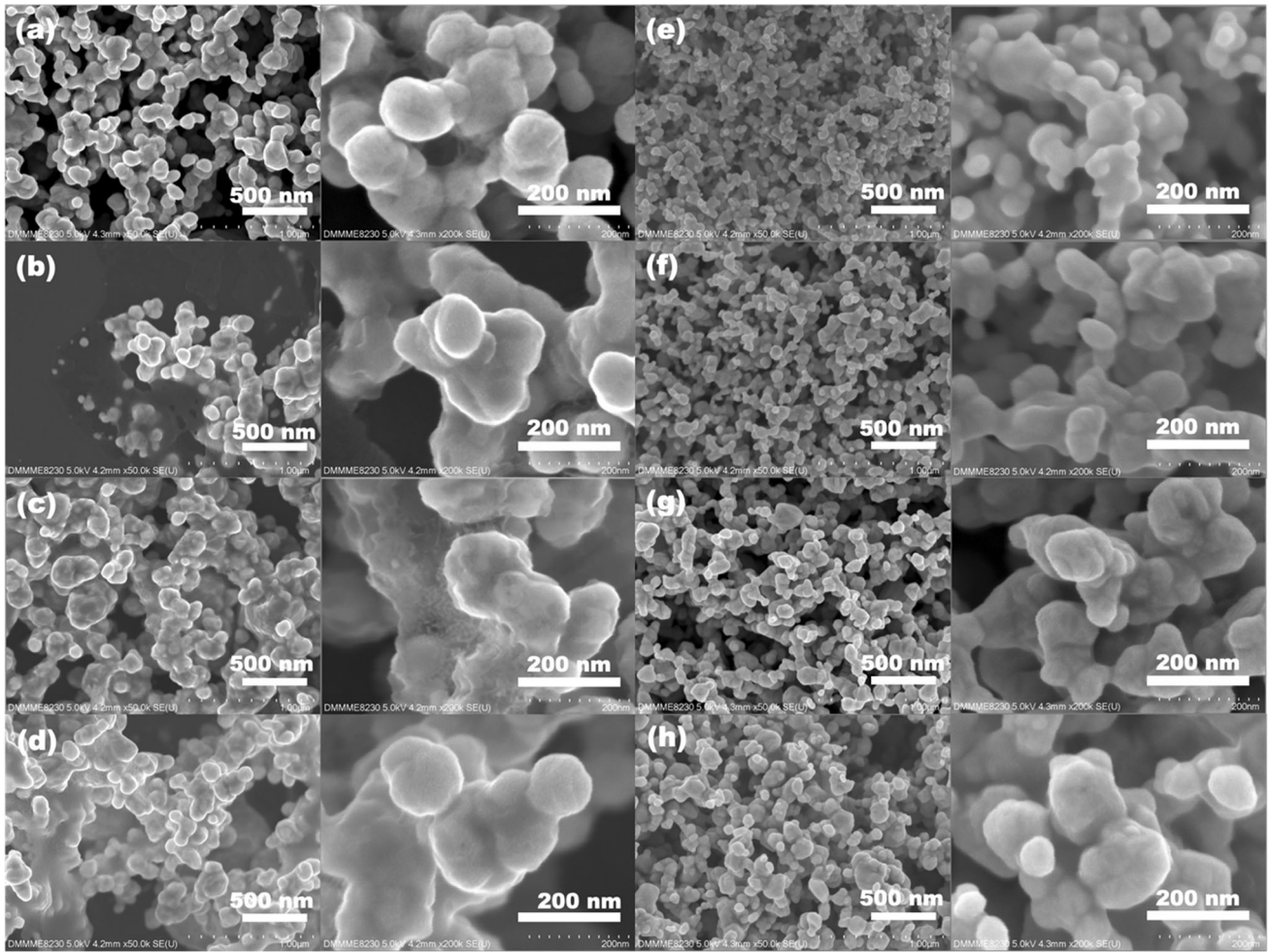


Fig. 7 Ag nanoparticles sintered using **a** 10, **b** 25, **c** 50, and **d** 75 mM LiCl solution, and **e** 10, **f** 25, **g** 50, and **h** 75 mM KCl solution. The magnification from left to right is 50,000× and 200,000× per sample

Table 3 Diameter of Ag nanoparticles fused using LiCl, NaCl, and KCl solutions at varying concentrations handwritten on glossy paper

Ag NP parameters	Fusing solution	Fusing solution concentration, mM				
		0	10	25	50	75
Diameter, nm	LiCl	24	134.8	164	168.3	189.4
% increase in diameter		0	461	583	601	689
Diameter standard deviation, %		–	26.70	23.96	25.53	17.21
Resistance, Ω		110,000	4.16	4.34	4.66	5.06
Resistance standard deviation, %		–	2.59	2.58	2.71	3.31
Diameter, nm	NaCl	24	103.7	195.6	197.4	221.7
% increase in diameter		0	332	715	723	824
Diameter standard deviation, %		–	24.55	42.39	19.37	53.75
Resistance, Ω		110,000	262.2	22.5	9.3	16.8
Resistance standard deviation, %		–	103.40	4.10	3.92	8.40
Diameter, nm	KCl	24	86.5	117.6	160	165.8
% increase in diameter		0	260	390	567	591
Diameter standard deviation, %		–	12.99	22.34	13.56	20.28
Resistance, Ω		110,000	2.96	3.28	3.34	4.68
Resistance standard deviation, %		–	1.87	2.22	2.06	3.40

seen in Fig. 8a–c. This value is consistent with the average diameter measured from the SEM images. The nanoparticles are mostly quasi-spherical, while some are faceted. Twinning lines were also present in some of the nanoparticles. The necks at the interface between the sintered nanoparticles are seen more clearly from the TEM images, which proves that sintering indeed occurred after the introduction of fusing solution (Fig. 8d, e). Lattice mismatch was also observed which may be due to the coalescence of nanoparticles with different lattice orientations.

In general, surfactants, such as polymers, can be chemically or physically adsorbed on the surface of nanoparticles to form a single or double-layer [34], which act as capping agents by creating repulsive forces between nanoparticles either by steric hindrance, electrostatic repulsion, or both. It was proposed that PAA is adsorbed on the Ag nanoparticle's surface via Ag–O coordination to provide electrostatic stabilization [10]. The presence of Cl^- ions on

the surface of Ag leads to the detachment of weakly anchored PAA chains [11]. Halides, such as Cl^- , are known to have strong interactions with Ag [11, 12]. Naturally, electrostatic repulsion would arise from the replacement of PAA molecules with Cl^- ions. There are two opposing forces present in the system: (1) van der Waals attractive forces between the surface of the particles and (2) the electrical double layer repulsive force which separates the particles via steric and electrostatic repulsive mechanisms. Stability is obtained if the repulsive force surpasses the van der Waals attractive forces [35]. It can be inferred that the electrostatic repulsion caused by Cl^- ions may not be enough to overcome the van der Waals attractive forces between nanoparticles. Coalescence of individual Ag nanoparticles then occurs to lower the high surface energy brought about by the desorption of PAA.

In addition to coalescence, the growth of nanoparticles also possibly involves Ostwald

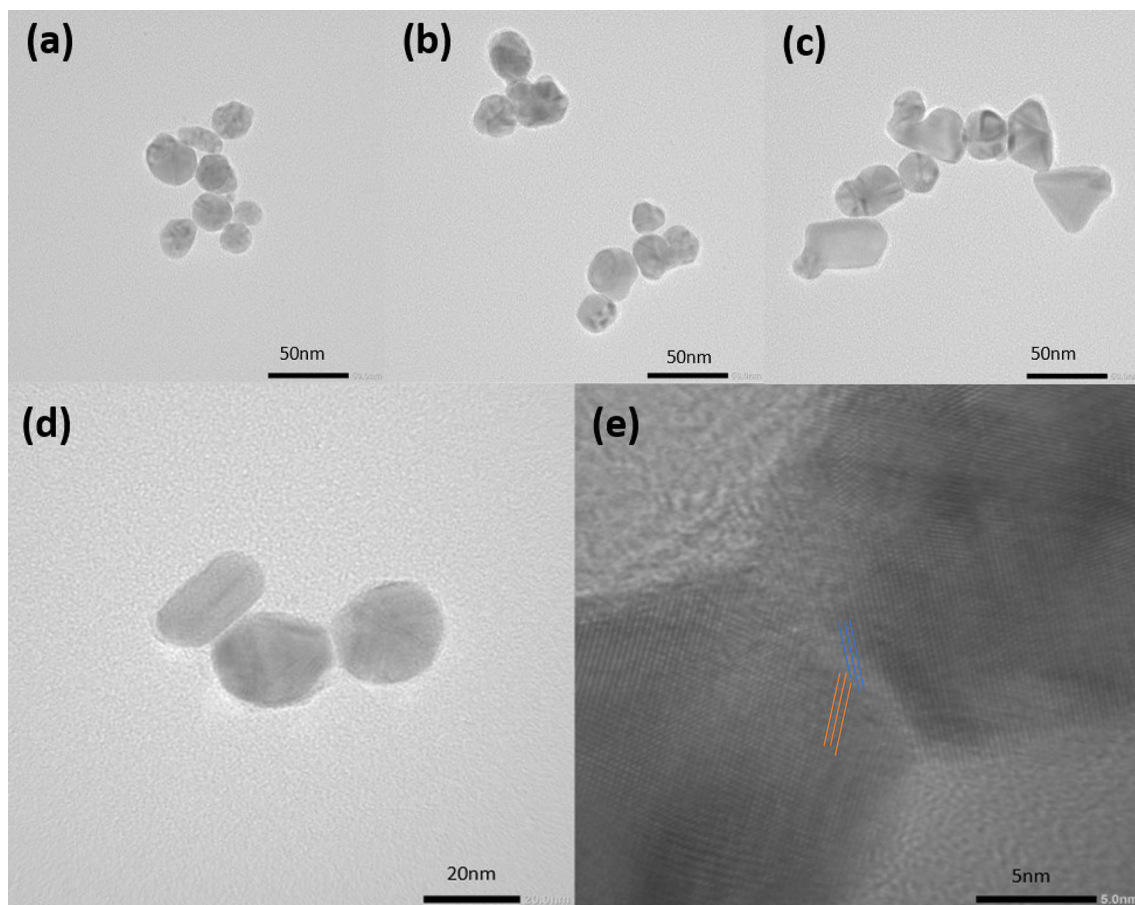


Fig. 8 (Color online) TEM images of **a** as-prepared and **b–e** sintered Ag nanoparticles showing necking. Lines indicate the direction of the lattice fringes in each particle

ripening due to the decrease in the total number of particles after sintering [36]. The driving force for Ostwald ripening is also the minimization of the surface energy of the system [37]. Anderson et al. examined the impact of stabilizer structure on the Ostwald ripening rate and indicated that steric length of the stabilizer molecule is the most important parameter in preventing Ostwald ripening. A shorter steric length generally results in an increased ripening rate [37]. Therefore, the replacement of PAA with Cl^- on the surface of Ag nanoparticles may have promoted Ostwald ripening due to shorter steric length.

Figure 9 shows the Raman spectra of as-prepared and fused Ag nanoparticles. Peaks at 1600 and 1387 cm^{-1} are characteristic of PAA molecule with 1600 cm^{-1} ascribed to the vibration of $\text{C}=\text{C}$ and 1387 cm^{-1} to $\text{O}-\text{C}-\text{O}$ vibrations. Both peaks became weak after treating the Ag nanoparticles with 50 mM NaCl solution, suggesting partial removal of PAA. The peak at 1004 cm^{-1} for fused Ag nanoparticles is ascribed to Ag molecule which was more prominent after treatment with the fusing solution. This may be due to the exposure of Ag upon removal of PAA molecules, which corresponds well with the proposed sintering mechanism. Results of the UV–Vis analysis showed an absorption peak at $425\text{--}437\text{ nm}$ for both supernatant solutions as seen in Fig. 9. These peaks are attributed to the surface plasmon resonance of Ag bound in Ag nanoparticles [38, 39]. The presence of these peaks in the supernatant solution may

be due to the presence of residual Ag nanoparticles even after decantation. The shouldering observed on the main peak of the supernatant after sintering may be due to impurities, i.e. sodium and chloride ions, introduced when the sintering solution was added.

To understand why PAA-Na is an effective stabilizer for Ag nanoparticles in this work, Ag nanoparticles were prepared using a normal PAA. Figure 10 shows the morphology of the Ag nanoparticles prepared with PAA before and after sintering using 50 mM NaCl. Ag nanoparticles with an average diameter of 32.6 nm were successfully synthesized using PAA. However, rods and other non-spherical particles were also present (Fig. 10a). The conductivity of Ag nanoparticles using PAA was also enhanced after mixing with 50 mM NaCl. This is evident from the decrease in the measured resistance from 226.0 to $41.7\text{ k}\Omega$. The standard deviation of the resistance values is about $10\text{--}15\%$ of the average value. Then again, the measured resistance values are significantly larger compared to the sample stabilized with PAA-Na even after sintering. Relative to the sintered Ag/PAA-Na nanoparticles, sintering was not extensive among the nanoparticles, which is possibly due to the different stabilization mechanisms provided by the two polymers. PAA provides mainly steric stabilization due to its weakly anionic, elongated structure, while PAA-Na provides electrosteric stabilization due to the presence of negatively charged carboxylate side chains. Steric stabilizers are relatively insensitive to the presence of

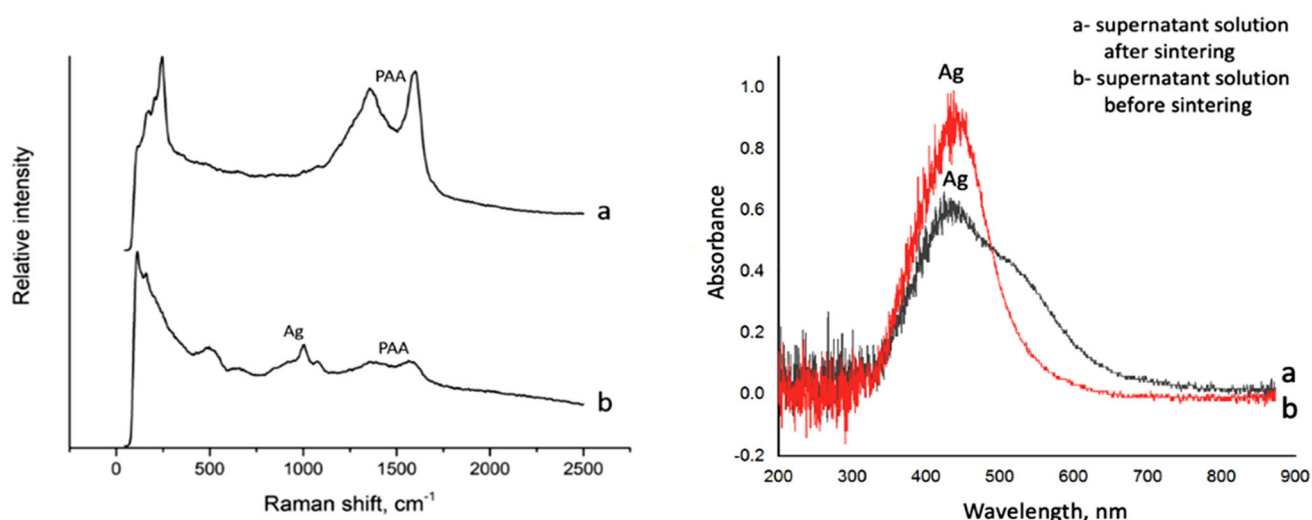


Fig. 9 (Color online) (LEFT) Raman spectra of **a** as-prepared and **b** fused Ag nanoparticles. (RIGHT) UV–Vis spectra of the supernatant solution **a** after and **b** before sintering

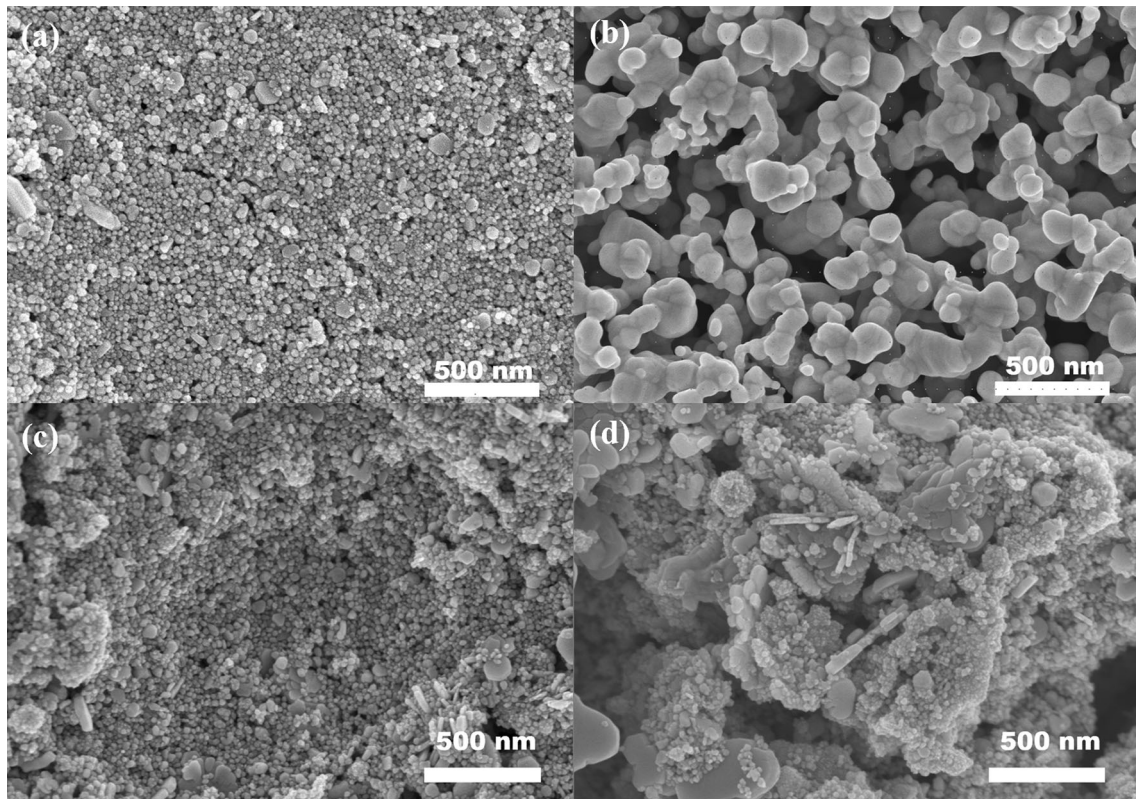


Fig. 10 SEM images of **a** as-synthesized and **b** sintered Ag nanoparticles using PAA-Na as a stabilizer and **c** as-synthesized and **d** sintered Ag nanoparticles using PAA as a stabilizer. Sintering was done using 50 mM NaCl solution

electrolytes than electrostatic stabilizers [40]. Further, PAA-Na is readily ionized in an aqueous solution to produce a negatively charged polymer molecule. Meanwhile, PAA ionization depends on the dilution of the solution [41]. This means that even with the same concentration, PAA-Na produces more charged molecules than PAA which may have resulted in a more effective stabilization of the synthesized nanoparticles.

4 Conclusions

In this study, sintering of Ag nanoparticles was done at room temperature. Sintering was performed via (1) mixing and (2) sequential printing methods. Mixing the as-prepared Ag nanoparticles with the sintering solution produced larger particles compared to the sample prepared via sequential printing. Room-temperature sintering may have been triggered by the introduction of electrolytic halide solutions in the system, which caused the destabilization and eventually the desorption of the polymer stabilizer. The

removal of the stabilizer led to the coalescence of Ag nanoparticles to lower the surface energy. Solutions containing anions with smaller ionic sizes tend to generate larger Ag particles and consequently, highly conductive written patterns. Meanwhile, solutions with larger cations tend to generate conductive inks with the lowest resistance values. Sintering also occurs more efficiently when PAA-Na salt was used compared to its neutral counterpart which is PAA. This can be due to the ionic nature of the salt counterpart which is more affected by the presence of electrolytic halide solutions.

Acknowledgements

The authors wish to thank the Department of Science and Technology through the Philippine Council for Industry, Energy, and Emerging Technology Research and Development (DOST-PCIEERD) under the research project entitled “Up-Scaled Synthesis of Metal Nanowires and their Application in Transparent Metal Nanowire Touch Panel” and the

Engineering Research and Development for Technology (DOST-ERDT) research grant for the financial support. The authors would also like to thank the Active Nanomaterial Synthesis and Devices Laboratory (ANSyD) through Dr. Candy C. Mercado for the use of the UV-Vis spectrometer. Dr. Balela would also like to acknowledge the Uratex Professorial Chair in Engineering through the University of the Philippines Engineering Research and Development Foundation, Inc. (UPERDFI).

Author contributions

BFYR: Conceptualization, Methodology, Investigation, Writing-original draft. MDLB: Conceptualization, Resources, Supervision, Writing-review and editing.

Funding

Funding was secured from the following agencies: Department of Science and Technology- Philippine Council for Industry, Energy, and Emerging Technology Research and Development (DOST-PCIEERD). DOST- Engineering Research and Development for Technology (ERDT).

Data availability

Available upon request to authors.

Declarations

Conflict of interest The authors declare that they do not have any conflict of interest/competing interest.

References

1. P. Sarobol et al., Additive manufacturing of hybrid circuits. *Annu. Rev. Mater. Res.* **46**, 41–62 (2016). <https://doi.org/10.1146/annurev-matsci-070115-031632>
2. A.J. Kell et al., Versatile molecular silver ink platform for printed flexible electronics. *ACS Appl. Mater. Interfaces* **9**(20), 17226–17237 (2017). <https://doi.org/10.1021/acsami.7b02573>
3. S.H. Ko, H. Pan, C.P. Grigoropoulos, C.K. Luscombe, J.M.J. Fr chet, D. Poulidakos, Air stable high resolution organic transistors by selective laser sintering of ink-jet printed metal nanoparticles. *Appl. Phys. Lett.* **90**(14), 141103 (2007). <https://doi.org/10.1063/1.2719162>
4. D.A. Kislov, Effect of plasmonic silver nanoparticles on the photovoltaic properties of graetzel solar cells. *Phys. Procedia* **73**, 114–120 (2015). <https://doi.org/10.1016/j.phpro.2015.09.130>
5. A. Ciesielski, K.M. Czajkowski, D. Switlik, Silver nanoparticles in organic photovoltaics: finite size effects and optimal concentration. *Sol. Energy* **184**, 477–488 (2019). <https://doi.org/10.1016/j.solener.2019.04.015>
6. F.M. Wolf, J. Perelaer, S. Stumpf, D. Bollen, F. Kriebel, U.S. Schubert, Rapid low-pressure plasma sintering of inkjet-printed silver nanoparticles for RFID antennas. *J. Mater. Res.* **28**(9), 1254–1261 (2013). <https://doi.org/10.1557/jmr.2013.73>
7. J.F. Salmer n et al., Properties and printability of inkjet and screen-printed silver patterns for RFID antennas. *J. Electron. Mater.* **43**(2), 604–617 (2014). <https://doi.org/10.1007/s11664-013-2893-4>
8. T.R. Allington, V. Johnson, Membrane touch switches: thick-film materials systems and processing options. *IEEE Trans. Compon. Hybrids Manuf. Technol.* **3**(4), 518–524 (1980). <https://doi.org/10.1109/TCHMT.1980.1135649>
9. J. Kim, J.H. Jong, W.S. Kim, Repeatedly bendable paper touch pad via direct stamping of silver nanoink with pressure-induced low-temperature annealing. *IEEE Trans. Nanotechnol.* **12**(6), 1139–1143 (2013). <https://doi.org/10.1109/TNANO.2013.2281326>
10. A. Russo, B.Y. Ahn, J.J. Adams, E.B. Duoss, J.T. Bernhard, J.A. Lewis, Pen-on-paper flexible electronics. *Adv. Mater.* **23**(30), 3426–3430 (2011). <https://doi.org/10.1002/adma.201101328>
11. S. Magdassi, M. Grouchko, O. Berezin, A. Kamyshny, Triggering the sintering of silver nanoparticles at room temperature. *ACS Nano* **4**(4), 1943–1948 (2010). <https://doi.org/10.1021/nn901868t>
12. M. Layani, M. Grouchko, S. Shemesh, S. Magdassi, Conductive patterns on plastic substrates by sequential inkjet printing of silver nanoparticles and electrolyte sintering solutions. *J. Mater. Chem.* **22**(29), 14349–14352 (2012). <https://doi.org/10.1039/c2jm32789a>
13. E.M. Datu, M.D.L. Balela, In situ electrochemical study of copper nanoparticles stabilized with food grade gelatin. *Key Eng. Mater.* **705**, 163–167 (2016)
14. M.D.L. Balela, K.L.S. Amores, Formation of highly antimicrobial copper nanoparticles by electroless deposition in water. *Sci. Diliman* **27**(2), 10–20 (2015)

15. M. Tan, L. de Jesus, K.L. Amores, E. Datu, D. Balela, Electroless deposition of copper nanostructures in aqueous solution. *Adv. Mater. Res.* **1043**, 114–118 (2014)
16. W. Cui, W. Lu, Y. Zhang, G. Lin, T. Wei, L. Jiang, Gold nanoparticle ink suitable for electric-conductive pattern fabrication using in ink-jet printing technology. *Colloids Surfaces A Physicochem. Eng. Asp.* **358**(1–3), 35–41 (2010). <https://doi.org/10.1016/j.colsurfa.2010.01.023>
17. K. Saha, S.S. Agasti, C. Kim, X. Li, V.M. Rotello, Gold nanoparticles in chemical and biological sensing. *Chem. Rev.* **112**(5), 2739–2779 (2012). <https://doi.org/10.1021/cr2001178>
18. D.C. Corsino, M.D.L. Balela, Room temperature sintering of printer silver nanoparticle conductive ink. *IOP Conf. Ser. Mater. Sci. Eng.* **264**(1), 012020 (2017). <https://doi.org/10.1088/1757-899X/264/1/012020>
19. N. De. Guzman, M.D. Balela, CuCl₂-mediated synthesis of silver nanowires for flexible transparent conducting films. *MATEC Web Conf.* **27**, 3–5 (2015). <https://doi.org/10.1051/mateconf/20152703007>
20. J.S. Kang, J. Ryu, H.S. Kim, H.T. Hahn, Sintering of inkjet-printed silver nanoparticles at room temperature using intense pulsed light. *J. Electron. Mater.* **40**(11), 2268–2277 (2011). <https://doi.org/10.1007/s11664-011-1711-0>
21. N. De. Guzman, M.D.L. Balela, Growth of ultralong Ag nanowires by electroless deposition in hot ethylene glycol for flexible transparent conducting electrodes. *J. Nanomater.* (2017). <https://doi.org/10.1155/2017/7896094>
22. T.H.J. Van Osch, J. Perelaer, A.W.M. De. Laat, U.S. Schubert, Inkjet printing of narrow conductive tracks on untreated polymeric substrates. *Adv. Mater.* **20**(2), 343–345 (2008). <https://doi.org/10.1002/adma.200701876>
23. S. Sivaramakrishnan, P.J. Chia, Y.C. Yeo, L.L. Chua, P.K.H. Ho, Controlled insulator-to-metal transformation in printable polymer composites with nanometal clusters. *Nat. Mater.* **6**(2), 149–155 (2007). <https://doi.org/10.1038/nmat1806>
24. D. Kim, S. Jeong, B.K. Park, J. Moon, Direct writing of silver conductive patterns: Improvement of film morphology and conductance by controlling solvent compositions. *Appl. Phys. Lett.* **89**(26), 87–90 (2006). <https://doi.org/10.1063/1.2424671>
25. J. Perelaer, B.J. De. Gans, U.S. Schubert, Ink-jet printing and microwave sintering of conductive silver tracks. *Adv. Mater.* **18**(16), 2101–2104 (2006). <https://doi.org/10.1002/adma.200502422>
26. K.A. Bogle, S.D. Dhole, V.N. Bhoraskar, Silver nanoparticles: synthesis and size control by electron irradiation. *Nanotechnology* **17**(13), 3204–3208 (2006). <https://doi.org/10.1088/0957-4484/17/13/021>
27. Y. Long, J. Wu, H. Wang, X. Zhang, N. Zhao, J. Xu, Rapid sintering of silver nanoparticles in an electrolyte solution at room temperature and its application to fabricate conductive silver films using polydopamine as adhesive layers. *J. Mater. Chem.* **21**(13), 4875–4881 (2011). <https://doi.org/10.1039/c0jm03838e>
28. M. Layani, S. Magdassi, Flexible transparent conductive coatings by combining self-assembly with sintering of silver nanoparticles performed at room temperature. *J. Mater. Chem.* **21**(39), 15378–15382 (2011). <https://doi.org/10.1039/c1jm13174e>
29. M. Grouchko, A. Kamyshny, C.F. Mihailescu, D.F. Anghel, S. Magdassi, Conductive inks with a ‘built-in’ mechanism that enables sintering at room temperature. *ACS Nano* **5**(4), 3354–3359 (2011). <https://doi.org/10.1021/nn2005848>
30. T. Öhlund, J. Örtengren, S. Forsberg, H.E. Nilsson, Paper surfaces for metal nanoparticle inkjet printing. *Appl. Surf. Sci.* **259**, 731–739 (2012). <https://doi.org/10.1016/j.apsusc.2012.07.112>
31. T. Öhlund, M. Hummelgård, H. Olin, Sintering inhibition of silver nanoparticle films via AgCl nanocrystal formation. *Nanomaterials* **7**(8), 1–13 (2017). <https://doi.org/10.3390/nano7080224>
32. J. Mähler, I. Persson, A study of the hydration of the alkali metal ions in aqueous solution. *Inorg. Chem.* **51**(1), 425–438 (2012). <https://doi.org/10.1021/ic2018693>
33. V.I. Volkov et al., Hydration and diffusion of h⁺, li⁺, na⁺, cs⁺ ions in cation-exchange membranes based on polyethylene-and sulfonated-grafted polystyrene studied by NMR technique and ionic conductivity measurements. *Membranes (Basel)* **10**(10), 1–14 (2020). <https://doi.org/10.3390/membranes10100272>
34. A.H. Lu, E.L. Salabas, F. Schüth, Magnetic nanoparticles: synthesis, protection, functionalization, and application. *Angew. Chem.—Int. Ed.* **46**(8), 1222–1244 (2007). <https://doi.org/10.1002/anie.200602866>
35. N. Ali, J.A. Teixeira, A. Addali, A review on nanofluids: fabrication, stability, and thermophysical properties. *J. Nanomater.* (2018). <https://doi.org/10.1155/2018/6978130>
36. T.W. Hansen, A.T. Delariva, S.R. Challa, A.K. Datye, Sintering of catalytic nanoparticles: particle migration or ostwald ripening? *Acc. Chem. Res.* **46**(8), 1720–1730 (2013). <https://doi.org/10.1021/ar3002427>
37. R. Anderson, R. Buscall, R. Eldridge, P. Mulvaney, P.J. Scales, Ostwald ripening of comb polymer stabilised Ag salt nanoparticles. *Colloids Surfaces A Physicochem. Eng. Asp.* **459**, 58–64 (2014). <https://doi.org/10.1016/j.colsurfa.2014.06.033>
38. A. Fahmy, W.H. Eisa, M. Yosef, A. Hassan, Ultra-thin films of poly(acrylic acid)/silver nanocomposite coatings for antimicrobial applications. *J. Spectrosc.* (2016). <https://doi.org/10.1155/2016/7489536>

39. R. Das, S.S. Nath, D. Chakdar, G. Gope, R. Bhattacharjee, Synthesis of silver nanoparticles and their optical properties. *J. Exp. Nanosci.* **5**(4), 357–362 (2010). <https://doi.org/10.1080/17458080903583915>
40. D. Rawlins, J. Kayes, Steric stabilization of suspensions. *Drug Dev. Ind. Pharm.* **6**(5), 427–440 (1980). <https://doi.org/10.3109/03639048009068715>
41. H. Markovitz, G.E. Kimball, The effect of salts on the viscosity of solutions of polyacrylic acid. *J. Colloid Sci.* **5**(2), 115–139 (1950). [https://doi.org/10.1016/0095-8522\(50\)90014-6](https://doi.org/10.1016/0095-8522(50)90014-6)

Publisher's Note Springer Nature remains neutral with regard to jurisdictional claims in published maps and institutional affiliations.